C. R. Mecanique 346 (2018) 449–459

Contents lists available at ScienceDirect

Comptes Rendus Mecanique

www.sciencedirect.com

Interaction of a conductive crack and of an electrode at a piezoelectric bimaterial interface

Oleg Onopriienko [a,b], Volodymyr Loboda [b,*], Alla Sheveleva [c], Yuri Lapusta [a]

[a] Université Clermont Auvergne, CNRS, SIGMA Clermont, Institut Pascal, F-63000 Clermont-Ferrand, France
[b] Department of Theoretical and Computational Mechanics, Oles Honchar Dnipro National University, Gagarin Av., 72, Dnipro 49010, Ukraine
[c] Department of Computational Mathematics, Oles Honchar Dnipro National University, Gagarin Av., 72, Dnipro 49010, Ukraine

ARTICLE INFO

Article history:
Received 24 December 2017
Accepted 8 April 2018
Available online 20 April 2018

Keywords:
Electrically conductive interface crack
Piezoelectric bimaterial
Electrode

ABSTRACT

The interaction of a conductive crack and an electrode at a piezoelectric bi-material interface is studied. The bimaterial is subjected to an in-plane electrical field parallel to the interface and an anti-plane mechanical loading. The problem is formulated and reduced, via the application of sectionally analytic vector functions, to a combined Dirichlet–Riemann boundary value problem. Simple analytical expressions for the stress, the electric field, and their intensity factors as well as for the crack faces' displacement jump are derived. Our numerical results illustrate the proposed approach and permit to draw some conclusions on the crack–electrode interaction.

1. Introduction

Interface cracks in multi-layered piezoelectric systems have attracted substantial interest from researchers since they can significantly reduce device functionality. A comprehensive review of crack problems arising in piezoelectric bimaterials is presented, e.g., in Govorukha et al. [1] including in-plane, anti-plane cracks and other problems. Without pretending to be exhaustive, we may note some important works related to the anti-plane interface crack problem in piezoelectric bimaterials.

Based on the integral equation approach, the anti-plane problems of a crack situated at the interface between piezoelectric layers or between a piezoelectric layer and an elastic layer were considered in works by Narita and Shindo [2], Soh et al. [3], Kwon and Lee [4], Li and Tang [5], Wang and Sun [6], Feng et al. [7] for both electrically permeable and electrically impermeable assumptions on the crack faces. The papers by Fil'shtinskii and Fil'shtinskii [8], Hou and Mei [9], Gao and Wang [10] are devoted to the consideration of anti-plane interface crack problems for a piezoelectric compound subjected to piecewise uniform out-of-plane mechanical loading combined with in-plane electric loading at infinity, and also line loading at an arbitrary point.

The anti-plane problem of three collinear interface cracks between dissimilar transversely isotropic piezoelectric materials subjected to electromechanical loading was analyzed by Choi and Shin [11] and Choi and Chung [12]. The problem of a three-layer structure constructed of a piezoelectric and two elastic strips cracked at the interface was analyzed by Narita and Shindo [13], Kwon and Lee [14].

* Corresponding author.
E-mail addresses: onopriienko.oleg@gmail.com (O. Onopriienko), loboda@mail.dsu.dp.ua (V. Loboda), Shevelevaae@dnu.dp.ua (A. Sheveleva), lapusta@sigma-clermont.fr (Y. Lapusta).

https://doi.org/10.1016/j.crme.2018.04.001
1631-0721/

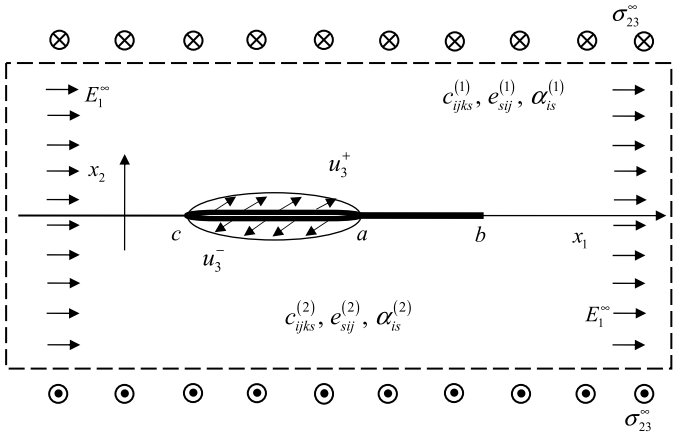

Fig. 1. Electrically conductive crack $c \le x_1 \le a$ approaching an electrode $a < x_1 < b$ at the interface $x_2 = 0$ between two piezoelectric materials. $u_3^{\pm}$ are unknown values of the crack faces' displacement.

The electroelastic interaction between a screw dislocation and a semi-infinite interface crack embedded in a two-phase piezoelectric medium has been investigated in the paper by Soh et al. [15]. Solutions for a screw dislocation interacting with a semi-infinite crack, finite crack, and edge crack between two bonded dissimilar piezoelectric materials were obtained in closed form by Wu et al. [16]. Many investigations were devoted to the anti-plane case of cracks moving along the interface of piezoelectric materials. The comprehensive review of such investigations is given in the recent paper by Nourazar and Ayatollahi [17].

In many cases, conducting interface cracks arise (Ru [18]). Such cracks were analyzed, e.g., by Beom and Atluri [19] and Loboda et al. [20] for "open" and contact zone crack models, respectively. Wang and Zhong [21] and also Wang et al. [22] studied a moving conducting crack at the interface of two dissimilar piezoelectric materials for an out-of-plane mechanical loading case. Lapusta et al. [23] analyzed a crack with mixed conditions at the crack faces. Although these cracks can interact with electrodes, to the best of our knowledge, this interaction has not been studied before. The present paper addresses this interesting and practically important case.

2. Problem formulation

Consider an electrically conductive crack $c \le x_1 \le a$ approaching an electrode $a < x_1 < b$ at the interface $x_2 = 0$ of a piezoelectric bimaterial (Fig. 1). The upper and lower components of the bimaterial are piezoceramics with poling direction x_3 and properties c_{ijks}, e_{sij}, α_{is}, where the mentioned values are stiffness, piezoelectric, and dielectric components, respectively.

We assume that a vector $\boldsymbol{P}^{\infty} = [\sigma_{23}^{\infty}, E_1^{\infty}]^{\intercal}$ is prescribed at infinity. We also assume the absence of stresses and electric field in the crack, the absence of the electric field as well as of stress and displacement jumps in the electrode zone and continuity conditions on the remaining part of the bimaterial interface. Thus, the boundary conditions at different parts of the interface have the form

$$\sigma_{23}^{(1)} = \sigma_{23}^{(2)} = 0, \qquad E_1^{(1)} = E_1^{(2)} = 0 \quad \text{for } c < x_1 < a \tag{1}$$

$$E_1^{(1)} = E_1^{(2)} = 0, \qquad \langle \varepsilon_{31} \rangle = 0, \qquad \langle \sigma_{23} \rangle = 0 \quad \text{for } a < x_1 < b \tag{2}$$

$$\langle \sigma_{23} \rangle = 0, \qquad \langle D_2 \rangle = 0, \qquad \langle \varepsilon_{31} \rangle = 0, \qquad \langle E_1 \rangle = 0 \quad \text{for } x_1 \notin (c, b) \tag{3}$$

Here and in the following, σ_{ij}, ε_{ij}, D_i, E_i denote stresses, strains, electric induction, and electric field, respectively. Recall that some basic piezoelectricity relations have the following form:

$$\sigma_{ij} = c_{ijks}\varepsilon_{ks} - e_{sij}E_s, \qquad D_i = e_{iks}\varepsilon_{ks} + \alpha_{is}E_s \tag{4}$$

Strains and electric field can be expressed using displacements u_i and electric potential φ in the form

$$\varepsilon_{ij} = \frac{1}{2}(u_{i,j} + u_{j,i}), \qquad E_i = -\varphi_{,i} \tag{5}$$

The equilibrium equations are:

$$\sigma_{ij,j} = 0, \qquad D_{i,i} = 0 \tag{6}$$

If an out-of-plane mechanical and in-plane electric loading is applied, we get a 2D problem with

$$u_1 = u_2 = 0, \qquad u_3 = u_3(x_1, x_2), \qquad \varphi = \varphi(x_1, x_2).$$

Using the conventional two-index notation for coefficients in (4) these relations take the form:

$$\begin{Bmatrix} \sigma_{3i} \\ D_i \end{Bmatrix} = \mathbf{R} \begin{Bmatrix} u_{3,i} \\ \varphi_{,i} \end{Bmatrix} \tag{7}$$

with $i = 1, 2$ and $\mathbf{R} = \begin{bmatrix} c_{44} & e_{15} \\ e_{15} & -\alpha_{11} \end{bmatrix}$.

Vectors

$$\boldsymbol{K} = [\sigma_{31}, D_1]^\intercal, \qquad \boldsymbol{u} = [u_3, \varphi]^\intercal, \qquad \boldsymbol{t} = [\sigma_{23}, D_2]^\intercal \tag{8}$$

are bound by the following relations:

$$\boldsymbol{K} = \mathbf{R}\boldsymbol{u}_{,1}, \qquad \boldsymbol{t} = \mathbf{R}\boldsymbol{u}_{,2} \tag{9}$$

As u_3 and φ are harmonic, they can be presented as a real part of an analytic function $\boldsymbol{\Phi}(z) = [\boldsymbol{\Phi}_1(z), \bar{\boldsymbol{\Phi}}_2(z)]^\intercal$ of complex variable $z = x_1 + \mathrm{i}x_2$

$$\boldsymbol{u} = 2\,\mathrm{Re}\,\boldsymbol{\Phi}(z) = \boldsymbol{\Phi}(z) + \bar{\boldsymbol{\Phi}}(\bar{z}) \tag{10}$$

We use the previous equations and derive:

$$\boldsymbol{t} = \mathbf{Q}\boldsymbol{\Phi}'(z) + \bar{\mathbf{Q}}\bar{\boldsymbol{\Phi}}'(\bar{z}), \qquad \boldsymbol{K} = -\mathrm{i}\mathbf{Q}\boldsymbol{\Phi}'(z) + \mathrm{i}\bar{\mathbf{Q}}\bar{\boldsymbol{\Phi}}'(\bar{z}) \tag{11}$$

where $\mathbf{Q} = \mathrm{i}\mathbf{R}$.

We also obtain:

$$\mathbf{v}' = \mathbf{A}\boldsymbol{\Phi}'(z) + \bar{\mathbf{A}}\bar{\boldsymbol{\Phi}}'(\bar{z}) \tag{12}$$

$$\boldsymbol{P} = \mathbf{B}\boldsymbol{\Phi}'(z) + \bar{\mathbf{B}}\bar{\boldsymbol{\Phi}}'(\bar{z}) \tag{13}$$

where

$$\mathbf{A} = \begin{bmatrix} 1 & 0 \\ Q_{21} & Q_{22} \end{bmatrix}, \qquad \mathbf{B} = \begin{bmatrix} Q_{11} & Q_{12} \\ 0 & 1 \end{bmatrix},$$

and

$$\mathbf{v}' = [u_3', D_2]^\intercal, \qquad \boldsymbol{P} = [\sigma_{23}, -E_1]^\intercal \tag{14}$$

Consider now a piezoelectric bi-material composed of two half-planes with an interface $x_2 = 0$ and apply Eqs. (12) and (13) to both components of the bimaterial.

$$\mathbf{v}^{(m)} = \mathbf{A}^{(m)}\boldsymbol{\Phi}^{(m)}(z) + \bar{\mathbf{A}}^{(m)}\bar{\boldsymbol{\Phi}}^{(m)}(\bar{z}), \qquad \boldsymbol{P}^{(m)} = \mathbf{B}^{(m)}\boldsymbol{\Phi}'^{(m)}(z) + \bar{\mathbf{B}}^{(m)}\bar{\boldsymbol{\Phi}}'^{(m)}(\bar{z}) \quad (m = 1, 2) \tag{15}$$

where $\boldsymbol{\Phi}^{(m)}(z)$ are arbitrary functions analytic in the regions 1 and 2, respectively.

According to continuity conditions $\boldsymbol{P}^{(1)} = \boldsymbol{P}^{(2)}$ through the interface $x_2 = 0$, we get:

$$\mathbf{B}^{(1)}\boldsymbol{\Phi}'^{(1)}(x_1 + \mathrm{i}0) - \bar{\mathbf{B}}^{(2)}\bar{\boldsymbol{\Phi}}'^{(2)}(x_1 + \mathrm{i}0) = \mathbf{B}^{(2)}\boldsymbol{\Phi}'^{(2)}(x_1 - \mathrm{i}0) - \bar{\mathbf{B}}^{(1)}\bar{\boldsymbol{\Phi}}'^{(1)}(x_1 - \mathrm{i}0) \tag{16}$$

The left- and right-hand sides of the last equation can be considered as the limit values of

$$\mathbf{B}^{(1)}\boldsymbol{\Phi}'^{(1)}(z) - \bar{\mathbf{B}}^{(2)}\bar{\boldsymbol{\Phi}}'^{(2)}(z) \quad \text{and} \quad \mathbf{B}^{(2)}\boldsymbol{\Phi}'^{(2)}(z) - \bar{\mathbf{B}}^{(1)}\bar{\boldsymbol{\Phi}}'^{(1)}(z) \tag{17}$$

which are analytic functions in the upper and lower planes, respectively.

We further obtain that functions (17) are equal to zero for any z from the corresponding half-plane,

$$\bar{\boldsymbol{\Phi}}'^{(2)}(z) = \left(\bar{\mathbf{B}}^{(2)}\right)^{-1}\mathbf{B}^{(1)}\boldsymbol{\Phi}'^{(1)}(z) \quad \text{for } x_2 > 0 \tag{18}$$

$$\bar{\boldsymbol{\Phi}}'^{(1)}(z) = \left(\bar{\mathbf{B}}^{(1)}\right)^{-1}\mathbf{B}^{(2)}\boldsymbol{\Phi}'^{(2)}(z) \quad \text{for } x_2 < 0 \tag{19}$$

and get the jump

$$\left\langle \mathbf{v}'(x_1) \right\rangle = \mathbf{v}'^{(1)}(x_1 + \mathrm{i}0) - \mathbf{v}'^{(2)}(x_1 - \mathrm{i}0) \tag{20}$$

of the vector function $\mathbf{v}'(x_1)$ over the interface. Using (15)

$$\mathbf{v}'^{(m)}(x_1 \pm \mathrm{i}0) = \mathbf{A}^{(m)}\boldsymbol{\Phi}'^{(m)}(x_1 \pm \mathrm{i}0) + \bar{\mathbf{A}}^{(m)}\boldsymbol{\Phi}'^{(m)}(x_1 \mp \mathrm{i}0),$$

and substituting in (20), one gets:

$$\langle \mathbf{v}'(x_1) \rangle = \mathbf{A}^{(1)}\boldsymbol{\Phi}'^{(1)}(x_1 + \mathrm{i}0) + \bar{\mathbf{A}}^{(1)}\bar{\boldsymbol{\Phi}}'^{(1)}(x_1 - \mathrm{i}0) - \mathbf{A}^{(2)}\boldsymbol{\Phi}'^{(2)}(x_1 - \mathrm{i}0) - \bar{\mathbf{A}}^{(2)}\bar{\boldsymbol{\Phi}}'^{(2)}(x_1 + \mathrm{i}0).$$

Finding further $\boldsymbol{\Phi}'^{(2)}(x_1 - \mathrm{i}0) = (\mathbf{B}^{(2)})^{-1}\bar{\mathbf{B}}^{(1)}\bar{\boldsymbol{\Phi}}'^{(1)}(x_1 - \mathrm{i}0)$ from (19) and substituting this expression together with (12) at $x_2 \to +0$ in the latest formula, leads to:

$$\langle \mathbf{v}'(x_1) \rangle = \mathbf{D}\boldsymbol{\Phi}'^{(1)}(x_1 + \mathrm{i}0) + \bar{\mathbf{D}}\bar{\boldsymbol{\Phi}}'^{(1)}(x_1 - \mathrm{i}0),$$

where $\mathbf{D} = \mathbf{A}^{(1)} - \bar{\mathbf{A}}^{(2)}(\bar{\mathbf{B}}^{(2)})^{-1}\mathbf{B}^{(1)}$. Introducing a new vector function,

$$\boldsymbol{W}(z) = \begin{cases} \mathbf{D}\boldsymbol{\Phi}'^{(1)}(z), & x_2 > 0, \\ -\bar{\mathbf{D}}\bar{\boldsymbol{\Phi}}'^{(1)}(z), & x_2 < 0, \end{cases} \tag{21}$$

the last relation can be written as

$$\langle \mathbf{v}'(x_1) \rangle = \boldsymbol{W}^+(x_1) - \boldsymbol{W}^-(x_1) \tag{22}$$

From the second relations (15), we have:

$$\boldsymbol{P}^{(1)}(x_1, 0) = \mathbf{B}^{(1)}\boldsymbol{\Phi}'^{(1)}(x_1 + \mathrm{i}0) + \bar{\mathbf{B}}^{(1)}\bar{\boldsymbol{\Phi}}'^{(1)}(x_1 - \mathrm{i}0) \tag{23}$$

Considering the fact that, on the base of (21),

$$\boldsymbol{\Phi}'^{(1)}(x_1 + \mathrm{i}0) = \mathbf{D}^{-1}\boldsymbol{W}(x_1 + \mathrm{i}0),$$
$$\bar{\boldsymbol{\Phi}}'^{(1)}(x_1 - \mathrm{i}0) = -\left(\bar{\mathbf{D}}^{-1}\right)^{-1}\boldsymbol{W}(x_1 - \mathrm{i}0),$$

and substituting these relations in (23) leads to

$$\boldsymbol{P}^{(1)}(x_1, 0) = \boldsymbol{S}\boldsymbol{W}^+(x_1) - \bar{\boldsymbol{S}}\boldsymbol{W}^-(x_1) \tag{24}$$

where $\boldsymbol{S} = \mathbf{B}^{(1)}\mathbf{D}^{-1}$. Simple calculations show that

$$\boldsymbol{S} = \left[\mathbf{A}^{(1)}\left(\mathbf{B}^{(1)}\right)^{-1} - \bar{\boldsymbol{A}}^{(2)}\left(\bar{\mathbf{B}}^{(2)}\right)^{-1}\right]^{-1} \tag{25}$$

It is worth to be mentioned that, for a case of a homogeneous material, this matrix becomes

$$\boldsymbol{S} = \frac{\mathrm{i}c_{44}}{2}\begin{bmatrix} 1 & 0 \\ 0 & (e_{15}^2 + c_{44}\alpha_{11})^{-1} \end{bmatrix}$$

and, in this particular case, completely coincides with the matrix $\mathrm{i}\boldsymbol{H}^{-1}$ obtained by method of Suo et al. [24]. For the case of a piezoceramics bimaterial studied here, we get that the matrix $\boldsymbol{S}$ has the following structure

$$\boldsymbol{S} = \begin{bmatrix} \mathrm{i}s_{11} & s_{12} \\ s_{21} & \mathrm{i}s_{22} \end{bmatrix} \tag{26}$$

where all s_{kl} $(k, l = 1, 2)$ are real.

3. Satisfied boundary conditions

Consider (24) in the following expanded form

$$\sigma_{23}^{(1)}(x_1, 0) = \mathrm{i}s_{11}W_1^+(x_1) + s_{12}W_2^+(x_1) + \mathrm{i}s_{11}W_1^-(x_1) - s_{12}W_2^-(x_1),$$
$$-E_1^{(1)}(x_1, 0) = s_{21}W_1^+(x_1) + \mathrm{i}s_{22}W_2^+(x_1) - s_{21}W_1^-(x_1) + \mathrm{i}s_{22}W_2^-(x_1) \tag{27}$$

in which (26) was taken into account. Combining the equations (27) one arrives at the presentations

$$\sigma_{23}^{(1)}(x_1, 0) - \mathrm{i}m_j E_1^{(1)}(x_1, 0) = t_j\left[F_j^+(x_1) + \gamma_j F_j^-(x_1)\right] \tag{28}$$

where

$$F_j(z) = W_2(z) + \mathrm{i}s_j W_1(z) \tag{29}$$

and $t_j = s_{12} - m_j s_{22}$, $\gamma_j = -(s_{12} + m_j s_{22})/t_j$, $s_j = (s_{11} + m_j s_{21})/t_j$, $m_{1,2} = \mp\sqrt{-\frac{s_{11}s_{12}}{s_{21}s_{22}}}$.

It follows from the last equations that $s_{1,2} = -m_{1,2}$, $\gamma_2 = 1/\gamma_1$, and the values $m_{1,2}$ are real.

Because, according to (26), $F_j^+(x_1) - F_j^-(x_1) = W_2^+(x_1) - W_2^-(x_1) + is_j[W_1^+(x_1) - W_1^-(x_1)]$, then using (22), one gets

$$\langle D_2(x_1,0)\rangle + is_j\langle u_3'(x_1,0)\rangle = F_j^+(x_1) - F_j^-(x_1) \tag{30}$$

It is sufficient to apply relations (28), (30) in the following analysis only for $j = 1$; therefore, assuming $j = 1$, the Eqs. (28) and (30) can be presented in the form:

$$\sigma_{23}^{(1)}(x_1,0) - im_1 E_1^{(1)}(x_1,0) = t_1\left[F_1^+(x_1) + \gamma_1 F_1^-(x_1)\right] \tag{31}$$

$$\langle D_2(x_1,0)\rangle + is_1\langle u_3'(x_1,0)\rangle = F_1^+(x_1) - F_1^-(x_1) \tag{32}$$

where $m_1 = -\sqrt{-\frac{s_{11}s_{12}}{s_{21}s_{22}}}$, $s_1 = -m_1$.

Presentations (31) and (32) are very convenient for the formulation and the resolution of the problems of linear relationship for piezoelectric bimaterials within a wide range of mixed interface conditions. One of such conditions is analyzed in this work.

Relations (22), (24) and, consequently, (31), (32) ensure satisfying equation $\boldsymbol{P}^{(1)}(x_1,0) = \boldsymbol{P}^{(2)}(x_1,0)$ for the whole interface and, accordingly, satisfying the first and fourth interface conditions (3). Further satisfaction of second and third conditions (3) provides the analyticity of the function $F_1(z)$ for the whole plane with a cut along the segment (c,b) of the interface. Satisfying the remaining boundary conditions (1) and (2) with use of (31) and (32), one gets the following equations

$$F_1^+(x_1) + \gamma_1 F_1^-(x_1) = 0 \quad \text{for } c < x_1 < a \tag{33}$$

$$\operatorname{Im}\left[F_1^+(x_1) + \gamma_1 F_1^-(x_1)\right] = 0, \qquad \operatorname{Im}\left[F_1^+(x_1) - F_1^-(x_1)\right] = 0 \quad \text{for } a < x_1 < b.$$

The last two relations lead to the equation

$$\operatorname{Im} F_1^{\pm}(x_1) = 0 \quad \text{for } a < x_1 < b \tag{34}$$

Taking into account that for $x_1 \notin (c,b)$ the relationships $F_1^+(x_1) = F_1^-(x_1) = F_1(x_1)$ are valid, it follows from Eq. (31)

$$(1+\gamma_1)t_1 F_1(x_1) = \sigma_{23}^{(1)}(x_1,0) - im_1 E_1^{(1)}(x_1,0) \quad \text{for } x_1 \to \infty.$$

Using the fact that the functions $F_1(z)$ are analytic in the whole plane cut along (c,b) and applying the conditions at infinity, one gets, from the last equation:

$$F_1(z)|_{z\to\infty} = \tilde{\sigma}_{23} - i\tilde{E}_1 \tag{35}$$

where $\tilde{\sigma}_{23} = \frac{\sigma_{23}^{\infty}}{r_1}$, $\tilde{E}_1 = \frac{m_1 E_1^{\infty}}{r_1}$, $r_1 = (1+\gamma_1)t_1$.

Relations (33) and (34) present the combined Dirichlet–Riemann boundary value problem. The solution to such a problem was found and applied to the analysis of a rigid stamp by Nahnein and Nuller [25]. Concerning the problem of an in-plane interface crack, this solution was developed by Loboda [26]. Using these results, an exact solution to the problems (33) and (34), satisfying the condition at infinity (35) as well as the condition of the displacement uniqueness and the absence of an electric charge in the crack region (Knish et al. [27]), can be written in the form

$$F_1(z) = P(z)X_1(z) + Q(z)X_2(z) \tag{36}$$

here

$$P(z) = C_1 z + C_2, \qquad Q(z) = D_1 z + D_2,$$

$$X_1(z) = ie^{i\chi(z)}/\sqrt{(z-c)(z-b)}, \qquad X_2(z) = e^{i\chi(z)}/\sqrt{(z-c)(z-a)},$$

$$\chi(z) = 2\varepsilon \ln\frac{\sqrt{(b-a)(z-c)}}{\sqrt{l(z-a)} + \sqrt{(a-c)(z-b)}}, \quad \varepsilon = \frac{1}{2\pi}\ln\gamma_1, \quad l = b-c,$$

$$C_1 = -\tilde{E}_1\cos\beta - \tilde{\sigma}_{23}\sin\beta, \qquad D_1 = \tilde{\sigma}_{23}\cos\beta - \tilde{E}_1\sin\beta,$$

$$C_2 = -\frac{c+b}{2}C_1 - \beta_1 D_1, \qquad D_2 = \beta_1 C_1 - \frac{c+a}{2}D_1,$$

with

$$\beta = \varepsilon\ln\frac{1-\sqrt{1-\lambda}}{1+\sqrt{1-\lambda}}, \qquad \beta_1 = \varepsilon\sqrt{(a-c)(b-c)}, \qquad \lambda = \frac{b-a}{l}.$$

Using the solution (36) together with formula (31), one gets

$$\sigma_{23}^{(1)}(x_1,0)-\mathrm{i}m_1E_1^{(1)}(x_1,0)=\left[\frac{Q(x_1)}{\sqrt{x_1-a}}+\frac{\mathrm{i}P(x_1)}{\sqrt{x_1-b}}\right]\frac{r_1\exp[\mathrm{i}\chi(x_1)]}{\sqrt{x_1-c}}\quad\text{for } x_1>b \tag{37}$$

$$\begin{aligned}\sigma_{23}^{(1)}(x_1,0)&=\frac{t_1P(x_1)}{\sqrt{(x_1-c)(b-x_1)}}\big[(1-\gamma_1)\cosh\varphi_0(x_1)+(1+\gamma_1)\sinh\varphi_0(x_1)\big]\\&\quad+\frac{t_1Q(x_1)}{\sqrt{(x_1-c)(x_1-a)}}\big[(1+\gamma_1)\cosh\varphi_0(x_1)+(1-\gamma_1)\sinh\varphi_0(x_1)\big]\quad\text{for } a<x_1<b\end{aligned} \tag{38}$$

where $\varphi_0(x_1)=2\varepsilon\tan^{-1}\sqrt{\frac{(a-c)(b-x_1)}{(b-c)(x_1-a)}}$.

Substituting the solution (36) into (32) gives the following formulas:

$$\big\langle D_2(x_1,0)\big\rangle+\mathrm{i}s_1\big\langle u_3'(x_1,0)\big\rangle=2\sqrt{\alpha}\left[\frac{P(x_1)}{\sqrt{b-x_1}}-\mathrm{i}\frac{Q(x_1)}{\sqrt{a-x_1}}\right]\frac{\exp[\mathrm{i}\varphi^*(x_1)]}{\sqrt{x_1-c}}\quad\text{for } c<x_1<a \tag{39}$$

$$\big\langle D_2(x_1,0)\big\rangle=\frac{2}{\sqrt{x_1-c}}\left[\frac{P(x_1)}{\sqrt{b-x_1}}\cosh\varphi_0(x_1)+\frac{Q(x_1)}{\sqrt{x_1-a}}\sinh\varphi_0(x_1)\right]\quad\text{for } a<x_1<b \tag{40}$$

where $\varphi^*(x_1)=2\varepsilon\ln\frac{\sqrt{(b-a)(x_1-c)}}{\sqrt{l(a-x_1)}+\sqrt{(a-c)(b-x_1)}}$, $\alpha=\frac{(\gamma_1+1)^2}{4\gamma_1}$.

It is worth to be mentioned that the obtained solution has an oscillating square root singularity at the left crack tip. However, it is very important that this solution is not oscillating at the right crack tip and, therefore, commonly used intensity factors can be introduced. Thus, we introduce further the following mechanical stress and electrical field intensity factors (IFs):

$$\begin{aligned}K_3&=\lim_{x_1\to a+0}\sqrt{2\pi(x_1-a)}\sigma_{23}^{(1)}(x_1,0),\\K_E&=\lim_{x_1\to b+0}\sqrt{2\pi(x_1-b)}E_1^{(1)}(x_1,0)\end{aligned} \tag{41}$$

Using Eq. (38) and taking into account that $\varphi_0(a)=\ln\sqrt{\gamma_1}$, one can find:

$$K_3=\frac{r_1Q(a)}{\sqrt{a-c}}\sqrt{\frac{2\pi}{\alpha}} \tag{42}$$

The intensity factor K_E can be inferred from the formula (37) and can be written in the form

$$K_E=-\frac{r_1}{m_1}\sqrt{\frac{2\pi}{l}}P(b) \tag{43}$$

It follows from Eq. (37) that the stress $\sigma_{23}^{(1)}(x_1,0)$ in the right neighborhood of the point b is finite, but Eq. (38) shows that in the left neighborhood of this point it is singular and the corresponding stress intensity factor (SIF)

$$K_{3b}=\lim_{x_1\to b-0}\sqrt{2\pi(b-x_1)}\sigma_{23}^{(1)}(x_1,0)$$

is equal to

$$K_{3b}=r_1\gamma_0\sqrt{\frac{2\pi}{l}}P(b)=-m_1\gamma_0K_E \tag{44}$$

where $\gamma_0=\frac{1-\gamma_1}{1+\gamma_1}$. Thus, we have only two independent IFs at the points a and b. These IFs can be presented in the form:

$$K_3=\sqrt{\frac{\pi l}{2\alpha}}\big[\sqrt{1-\lambda}\big(\sigma_{23}^{\infty}\cos\beta-m_1E_1^{\infty}\sin\beta\big)-2\varepsilon\big(\sigma_{23}^{\infty}\sin\beta+m_1E_1^{\infty}\cos\beta\big)\big] \tag{45}$$

$$K_E=\frac{1}{m_1}\sqrt{\frac{\pi l}{2}}\big[\big(\sigma_{23}^{\infty}\sin\beta+m_1E_1^{\infty}\cos\beta\big)+2\varepsilon\sqrt{1-\lambda}\big(\sigma_{23}^{\infty}\cos\beta-m_1E_1^{\infty}\sin\beta\big)\big] \tag{46}$$

It is worth to be mentioned that the identity

$$\alpha K_3^2+m_1^2K_E^2=\frac{\pi l}{2}\frac{(1-\lambda)(1+4\varepsilon^2)^2}{1+4\varepsilon^2-\lambda}\big[\big(\sigma_{23}^{\infty}\big)^2+m_1^2\big(E_1^{\infty}\big)^2\big] \tag{47}$$

is valid.

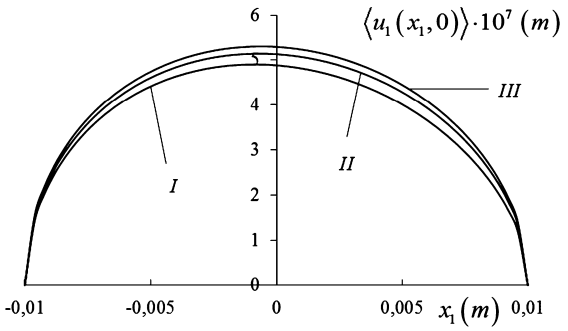

Fig. 2. Tangential displacement jump along the conductive crack for $E_1^\infty = 2 \cdot 10^4$ V/m.

Using of equation (39) for $x_1 \to a - 0$ permits to obtain the following expressions of $\langle u_3' \rangle$ via the SIF K_3:

$$\langle u_3'(x_1, 0)\rangle = -\frac{2\alpha}{r_1 s_1} \frac{K_3}{\sqrt{2\pi(a - x_1)}} \quad \text{for } x_1 \to a - 0 \tag{48}$$

According to (48), the derivative of the displacement jump at the crack tip a is proportional to the SIF K_3. To confirm the validity of the obtained solution, let us suppose that the electrode is absent and the only interface crack is situated along $c < x_1 < a$. In this case, the problem of the linear relationship

$$F_1^+(x_1) + \gamma_1 F_1^-(x_1) = 0 \quad \text{for } c < x_1 < a \tag{49}$$

follows from (1), (31) and the conditions at infinity (35) are valid.

This problem is relatively simple and its solution can be easily found with use of Muskhelishvili [28] in the form

$$F(z) = (\tilde{\sigma}_{23} - \mathrm{i}\tilde{E}_1) \frac{z - (a + c)/2 - \mathrm{i}\varepsilon l}{\sqrt{(z - c)(z - a)}} \left(\frac{z - c}{z - a}\right)^{\mathrm{i}\varepsilon} \tag{50}$$

The stress and electric field at the interface are obtained with use of (31) as follows

$$\sigma_{23}^{(1)}(x_1, 0) - \mathrm{i}m_1 E_1^{(1)}(x_1, 0) = \left(\sigma_{23}^\infty - \mathrm{i}m_1 E_1^\infty\right) \frac{x_1 - (a + c)/2 - \mathrm{i}\varepsilon l}{\sqrt{(x_1 - c)(x_1 - a)}} \left(\frac{x_1 - c}{x_1 - a}\right)^{i\varepsilon} \quad \text{for } x_1 > a \tag{51}$$

Consider for comparison the formula (37) for $b \to a$, i.e. for the limiting case of electrode length tending to 0. Taking into account that, for $b \to a$,

$$\frac{Q(x_1)}{\sqrt{x_1 - a}} + \frac{\mathrm{i}P(x_1)}{\sqrt{x_1 - b}} = \frac{x_1 - (a + c)/2 - \mathrm{i}\varepsilon l}{\sqrt{x_1 - a}} (D_1 + \mathrm{i}C_1),$$
$$D_1 + iC_1 = \left(\sigma_{23}^\infty - im_1 E_1^\infty\right) \exp(-\mathrm{i}\beta)/r_1$$

and

$$\exp\left[\mathrm{i}\chi(x_1) - \beta\right] = \left(\frac{x_1 - c}{x_1 - a}\right)^{\mathrm{i}\varepsilon},$$

we arrive exactly at Equation (51). This fact confirms the correctness of the solution (36) for the combination of a crack and an electrode at it continuation. Moreover, it shows that the presence of the electrode transforms the oscillating singularity at the tip a of an individual interface crack into two square root singularities at the points a and b.

4. Numerical results and discussion

We performed calculations for a bimaterial with the following characteristics (Wang et al. [22]): $c_{44}^{(1)} = 35.3 \cdot 10^9$ Pa, $e_{15}^{(1)} = 17 \frac{C}{m^2}$, $\alpha_{11}^{(1)} = 15.1 \cdot 10^{-9} \frac{C}{V \cdot m}$, $c_{44}^{(2)} = 42.47 \cdot 10^9$ Pa, $e_{15}^{(2)} = -0.48 \frac{C}{m^2}$, $\alpha_{11}^{(2)} = 0.0757 \cdot 10^{-9} \frac{C}{V \cdot m}$. The calculated tangential crack opening $\langle u_3(x_1, 0)\rangle$ for $c = -10$ mm, $a = 10$ mm, $\sigma_{23}^\infty = 1$ MPa is displayed in Figs. 2 and 3 for $E_1^\infty = 2 \cdot 10^4$ V/m and $E_1^\infty = 175781.47$ V/m, respectively. Figs. 4 and 5 show results for stresses $\sigma_{23}^{(1)}(x_1, 0)$ in the electrode zone for the same electric loads. Stresses $\sigma_{23}^{(1)}(x_1, 0)$ on the electrode continuation for the same electric loads are shown in Figs. 6 and 7. In all these figures, lines I, II and III correspond, respectively, to $b = 12$ mm, 16 mm, and 20 mm.

It can be seen from Figs. 2, 4 and 6 that, for a relatively small value of $E_1^\infty = 2 \cdot 10^4$ V/m, the dependence of the crack opening and stresses on the electrode length is rather small. By the way, for $E_1^\infty = 0$, this dependence is almost absent.

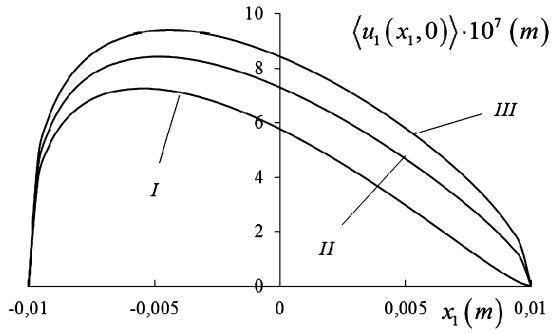

Fig. 3. Tangential displacement jump along the conductive crack for $E_1^{\infty} = 175781.47$ V/m.

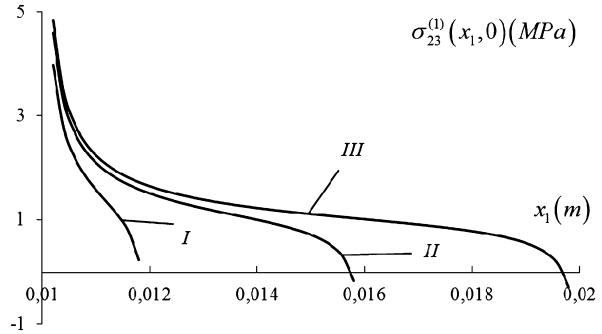

Fig. 4. Shear stress variation along the electrode zone for $E_1^{\infty} = 2 \cdot 10^4$ V/m.

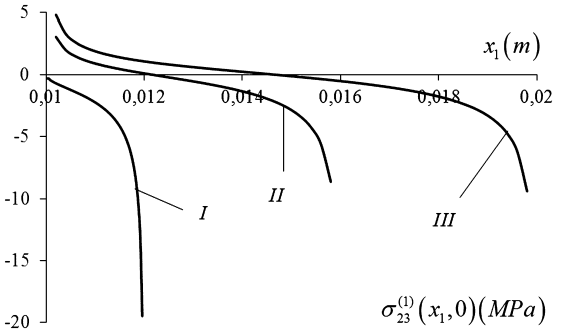

Fig. 5. Shear stress variation along the electrode zone for $E_1^{\infty} = 175781.47$ V/m.

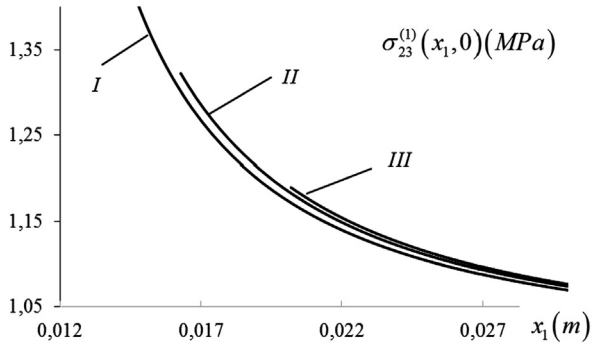

Fig. 6. Behavior of the shear stress at the electrode continuation for $E_1^{\infty} = 2 \cdot 10^4$ V/m.

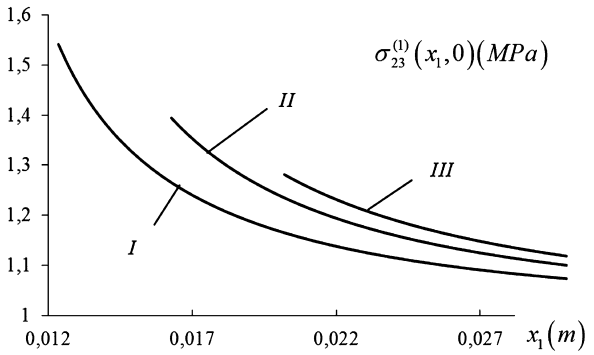

Fig. 7. Behavior of the shear stress at the electrode continuation for $E_1^\infty = 175781.47$ V/m.

Table 1
Stress and electric field intensity factors for different electrode lengths and the intensity of electric field.

b(m)	$K_3(\text{Pa}\cdot\sqrt{m})$		$K_E(V/\sqrt{m})$	
	$E_1^\infty = 2\cdot 10^4$	$E_1^\infty = 175781.47$	$E_1^\infty = 2\cdot 10^4$	$E_1^\infty = 175781.47$
0.012	153,331	≈ 0	2476.4	33,595.2
0.016	146,772	101,991	1337.0	33,213.2
0.020	138,234	142,244	912.35	32,850.1

Table 2
The variation of stress and electric field intensity factors for $b = 0.016$ m, $\sigma_{23}^\infty = 1$ MPa and different intensities of the electric field.

E_1^∞ (V/m)	K_3 $(\text{Pa}\cdot\sqrt{m})$	K_E $(V/\sqrt{m})$
−7372.95	151,891	≈ 0
$-3\cdot 10^3$	147,536	793
0	146,772	1337
$1\cdot 10^5$	121,297	19,471
$2.5\cdot 10^5$	83,083.3	46,671.9
576,131	≈ 0	105,812

For all cases presented in the Figures, except for lines I of Figs. 3, 5 and 7, the intensity factors K_3 and K_E differ from 0. This means that $\langle u_3'(x_1,0)\rangle$ is singular for $x_1 \to a-0$ and that $\sigma_{23}^{(1)}(x_1,0)$ is singular at both internal ends of $[a,b]$ for all mentioned cases. The lines I of Figs. 3, 5 and 7 correspond to the case where $K_3 = 0$. In this case, the crack closes smoothly at the point a (Fig. 3) and the stress $\sigma_{23}^{(1)}(x_1,0)$ tends to zero at this point. It is worth also noting that the stress $\sigma_{23}^{(1)}(x_1,0)$ is always finite for $x_1 \to b+0$ (Figs. 6, 7).

The intensity factors for the cases presented in Figs. 2–5 are given in Table 1. It can be seen from this Table that the stress intensity factor K_3 slightly decreases with growing the electrode length for $E_1^\infty = 2\cdot 10^4$ V/m, whilst it increases fast from zero to a rather large value for $E_1^\infty = 175781.47$ V/m. On the other hand, the electric intensity factor K_E varies insignificantly with growing values of λ for both mentioned values of E_1^∞.

The dependence of stress and electrical intensity factors on E_1^∞ are shown in Table 2 for $b = 0.016$ m and $\sigma_{23}^\infty = 1$ MPa. It can be seen that the variations of both K_3 and K_E on the electric field are rather essential. Moreover, the values of E_1^∞ for which K_3 or K_E became equal to zero are found and presented in the last and second lines of the table, respectively.

It follows from the obtained results displayed in Figs. 2–7, in Table 1, and especially in Table 2 that the electric field essentially influences the stress and displacement magnitudes as well as the stress and electric intensity factors. Particularly, due to the variation of E_1^∞, the SIF K_3 can be significantly decreased and even reduced to zero. On the other hand, very small negative values of E_1^∞ reduce to zero the IF of the electric field K_E.

Note finally that the SIF K_3 plays the most important role in this study. It defines the possibility of crack propagation. The variation of this SIF with respect to the position of the point b, defining the electrode length, is shown in Fig. 8 for the same material as in Figs. 2–7 and $c = -10$ mm, $a = 10$ mm. Lines I, II and III are drawn for E_1^∞ equal to 0, 1.0×10^5 V/m, and 2.0×10^5 V/m, respectively. It can be seen from this Figure that, for $E_1^\infty = 0$, the SIF K_3 is almost independent of the electrode length and, only for very small electrode lengths, some deviation from an almost straight line can be observed. This deviation can be explained by the transformation of the square root singularity at the point a into the oscillating singularity for $b \to a$ (see formulas (49), (51)). However, for a non-zero E_1^∞ (lines II and III), the dependence of K_3 from the electrode length becomes rather essential, especially for small values of b. It should be also noted that, for each of

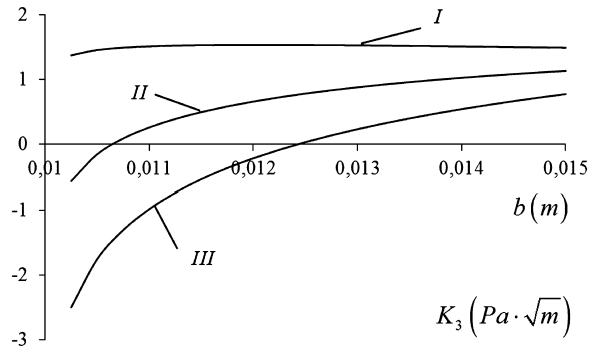

Fig. 8. Variation of the SIF K_3 with respect to the electrode length and the intensity of the external electric field.

the mentioned E_1^{∞}, there exists an electrode length for which the SIF K_3 transforms into zero and the danger of the crack development for such magnitudes of b vanishes.

5. Conclusion

The formulation of the problem of a conductive crack interacting with an electrode under an in-plane electrical field parallel to the crack faces and under out-of-plane mechanical load is analyzed. Presentations (31), (32) of the required electromechanical characteristics via sectionally analytic vector functions are constructed. Based upon these presentations, a combined Dirichlet–Riemann boundary value problem (33), (34) is formulated. An exact analytical solution to this problem is given for any crack and electrode length. Some analytical expressions (34)–(37) for stress, electric field, and their intensity factors as well as for the mechanical and electrical displacement jumps of the crack faces are presented. The correctness of the obtained solution is confirmed by its comparison in the limiting case with the well-known solution for a single interface crack.

In Figs. 2–7, the variations of the mentioned quantities along the appropriate parts of the material interface are illustrated for certain materials combination and for different relations between the crack and electrode lengths. The stress and electric field intensity factors corresponding to the results of Figs. 2–7 are given in Table 1. The dependence of the stress and electrical intensity factors on the magnitude of the electric field at infinity are shown in Table 2 for certain values of the external mechanical loading and of the coefficient between the crack and the electrode lengths. In particular, the values of the applied electric field inducing zero mechanical or electric intensity factors are distinguished in this Table. Special attention is devoted to the stress intensity factor K_3, which defines the possibility of crack propagation. Its variation with respect to the electrode length and the intensity of the electric field is demonstrated in Fig. 8. It particularly follows from this Figure that K_3 is almost independent of the electrode length for zero external electric field, but changing this field calls the dependence of K_3 on the mentioned length.

The analytical analysis and their numerical illustration induces some qualitative conclusions between which the most important are the following:

- due to the presence of an electrode at the crack continuation, the square root oscillating singularity at the tip of an individual interface crack transforms into two conventional square root singularities at the electrode ends;
- the influence of the electrode on the electromechanical characteristics of an interface crack is almost insensitive for zero external electric field, but it becomes rather susceptible in the opposite case.

Acknowledgements

This work has been carried out within the framework of the Transversal Program of the Pascal Institute (UMR CNRS 6602), Division “Materials and Multiscale Modeling”, of the Excellence Laboratory LabEx IMobS3 (ANR-10-LABX-16-01) (supported by the French program “Investissement d’avenir” and managed by the French National Research Agency (ANR), the European Commission (Auvergne FEDER funds) and the “Région Auvergne”), and, also, of the project CAP 20-25, Axis 2, Theme “Usine du futur”, which is gratefully acknowledged.

References

[1] V. Govorukha, M. Kamlah, V. Loboda, Y. Lapusta, Interface cracks in piezoelectric materials, Smart Mater. Struct. 25 (2016), 023001 (20 p.).
[2] F. Narita, Y. Shindo, The interface crack problem for bonded piezoelectric and orthotropic layers under antiplane shear loading, Int. J. Fract. 98 (1999) 87–101.
[3] A.K. Soh, D.N. Fang, K.L. Lee, Analysis of a bi-piezoelectric ceramic layer with an interfacial crack subjected to anti-plane shear and in-plane electric loading, Eur. J. Mech. A, Solids 19 (2000) 961–977.
[4] J.H. Kwon, K.Y. Lee, Interface crack between piezoelectric and elastic strips, Arch. Appl. Mech. 70 (2000) 707–714.

[5] X.F. Li, G.J. Tang, Antiplane interface crack between two bonded dissimilar piezoelectric layers, Eur. J. Mech. A, Solids 22 (2003) 231–242.
[6] B.L. Wang, Y.G. Sun, Out-of-plane interface cracks in dissimilar piezoelectric materials, Arch. Appl. Mech. 74 (2004) 2–15.
[7] F.X. Feng, K.Y. Lee, Y.D. Li, Multiple cracks on the interface between a piezoelectric layer and an orthotropic substrate, Acta Mech. 221 (2011) 297–308.
[8] L.A. Fil'shtinskii, M.L. Fil'shtinskii, Anti-plane deformation of a composite piezoceramic space with interphase crack, Int. Appl. Mech. 33 (1997) 655–659.
[9] M. Hou, F. Mei, Problems of antiplane strain of electrically permeable cracks between bonded dissimilar piezoelectric materials, Chin. Sci. Bull. 43 (1998) 341–345.
[10] C.F. Gao, M.Z. Wang, General treatment of mode III interfacial crack problems in piezoelectric materials, Arch. Appl. Mech. 71 (2001) 296–306.
[11] S.R. Choi, J.K. Shin, Three collinear antiplane interfacial cracks in dissimilar piezoelectric materials, Int. J. Fract. 179 (2013) 237–244.
[12] S.R. Choi, I. Chung, Analysis of three collinear antiplane interfacial cracks in dissimilar piezoelectric materials under non-self equilibrated electromechanical loadings on a center crack, J. Mech. Sci. Technol. 27 (2013) 3097–3101.
[13] F. Narita, Y. Shindo, Layered piezoelectric medium with interface crack under anti-plane shear, Theor. Appl. Fract. Mech. 30 (1998) 119–126.
[14] J.H. Kwon, K.Y. Lee, Interface crack between piezoelectric and elastic strips, Arch. Appl. Mech. 70 (2000) 707–714.
[15] A.K. Soh, J.X. Liu, D.N. Fang, A screw dislocation interacting with an interfacial crack in two dissimilar piezoelectric media, Phys. Status Solidi B 232 (2002) 273–282.
[16] X.F. Wu, S. Cohn, Y.A. Dzenis, Screw dislocations interacting with interfacial and interface cracks in piezoelectric biomaterials, Int. J. Eng. Sci. 41 (2003) 667–682.
[17] M. Nourazar, M. Ayatollahi, Multiple moving interfacial cracks between two dissimilar piezoelectric layers under electromechanical loading, Smart Mater. Struct. 25 (2016) 075011, 14 pp.
[18] C.Q. Ru, Electrode–ceramic interfacial cracks in piezoelectric multilayer materials, ASME J. Appl. Mech. 67 (2000) 255–261.
[19] H.G. Beom, S.N. Atluri, Conducting cracks in dissimilar piezoelectric media, Int. J. Fract. 118 (2002) 285–301.
[20] V. Loboda, A. Sheveleva, Y. Lapusta, An electrically conducting interface crack with a contact zone in a piezoelectric bimaterial, Int. J. Solids Struct. 51 (2014) 63–73.
[21] X. Wang, Z. Zhong, A conducting arc crack between a circular piezoelectric inclusion and an unbounded matrix, Int. J. Solids Struct. 39 (2002) 5895–5911.
[22] X. Wang, Z. Zhong, F.L. Wu, A moving conducting crack at the interface of two dissimilar piezoelectric materials, Int. J. Solids Struct. 40 (2003) 2381–2399.
[23] Y. Lapusta, O. Onopriienko, V. Loboda, An interface crack with partially electrically conductive crack faces under antiplane mechanical and in-plane electric loadings, Mech. Res. Commun. 81 (2017) 38–43.
[24] Z. Suo, C.-M. Kuo, D.M. Barnett, J.R. Willis, Fracture mechanics for piezoelectric ceramics, J. Mech. Phys. Solids 40 (1992) 739–765.
[25] E.L. Nakhmein, B.M. Nuller, Contact between an elastic half-plane and a partly separated stamp, J. Appl. Math. Mech. 50 (4) (1986) 507–515.
[26] V.V. Loboda, The quasi-invariant in the theory of interface cracks, Eng. Fract. Mech. 44 (1993) 573–580.
[27] P. Knysh, V. Loboda, F. Labesse-Jied, Y. Lapusta, An electrically charged crack in a piezoelectric material under remote electromechanical loading, Lett. Fract. Micromech. 175 (1) (2012) 87–94.
[28] N.I. Muskhelishvili, Some Basic Problems of Mathematical Theory of Elasticity, Noordhoff International Publishing, Leyden, The Netherlands, 1977.